Article

Not peer-reviewed version

Physicochemical Characteristics and Antimicrobial Efficacy of Plasma-Activated Water Produced by an Air-Operated Coaxial DBD Plasma

F. S. Miranda *, V. K. F. Tavares , Marcelo Pego Gomes , Nilton Neto , W. Chiappim *, Gilberto Petraconi , Rodrigo Pessoa , Cristiane Koga-Ito

Posted Date: 3 November 2023

doi: 10.20944/preprints202311.0229.v1

Keywords: Cold atmospheric plasma; Dielectric Barrier Discharge; Plasma-activated liquids; Plasma medicine; Staphylococcus aureus; Escherichia coli; Candida albicans

Article

Physicochemical Characteristics and Antimicrobial Efficacy of Plasma-Activated Water Produced by an Air-Operated Coaxial DBD Plasma

F. S. Miranda [1,2,*], V. K. F. Tavares [1], M. P. Gomes [2], N. F. Azevedo Neto [1], W. Chiappim [4,*], G. Petraconi [2], R. S. Pessoa [2] and C. Y. Koga-Ito [1,3]

[1] Department of Environment Engineering, Institute of Science and Technology, São Paulo State University (UNESP), São José dos Campos 12247-016, Brazil; f.miranda@unesp.br
[2] Plasmas and Processes Laboratory, Department of Physics, Aeronautics Institute of Technology, Praça Marechal Eduardo Gomes 50, São José dos Campos 12228-900, Brazil; rodrigospessoa@gmail.com
[3] Science Applied to Oral Health, Graduate Program of Institute of Science and Technology, UNESP, São José dos Campos 12245-000, Brazil; cykogaito@gmail.com
[4] Laboratory of Plasmas and Applications, Department of Physics, Faculty of Engineering and Sciences, São Paulo State University (UNESP), Guaratinguetá 12516-410, Brazil; william.chiappim@unesp.br
* Correspondence: f.miranda@unesp.br (F.S.M.), william.chiappim@unesp.br (W.C.)

Abstract: In this study, Plasma-Activated Water (PAW) was synthesized using a coaxial Dielectric Barrier Discharge (DBD) reactor, benefiting from the elevated capacity of air-flow-assisted DBD discharges to enhance nitrogen-based species concentration. By manipulating operational parameters, including gas flow rate, activation time, and DI water volume, we achieved significant concentrations of Reactive Oxygen and Nitrogen Species (RONS). As a result, the PAW obtained displayed pronounced physicochemical attributes: a pH of 2.06, an ORP of 275mV, conductivity of 3mS/cm, and TDS of 1200 mg/L. A pivotal aspect of this research was the evaluation of the reactor's efficiency, as indicated by metrics like the specific input energy and ozone efficiency yield. The antimicrobial potential of the PAW was also assessed against pathogenic microbes, with remarkable reductions in viability for both *Staphylococcus aureus* and *Escherichia coli* (99.99%) and a more moderate decrease for *Candida albicans* (37%). These findings underscore the capability of the coaxial DBD reactor in crafting high-quality PAW with significant antimicrobial properties, necessitating further studies to validate its broad-spectrum and safe application.

Keywords: cold atmospheric plasma; dielectric barrier discharge; plasma-activated liquids; plasma medicine; *Staphylococcus aureus*; *Escherichia coli*; *Candida albicans*

1. Introduction

Antimicrobial resistance is a major global concern, complicating the treatment of infectious diseases [1]. In recent years, technological advancements have fostered the development of novel antimicrobial alternatives. One such promising innovation is Low Temperature Atmospheric Pressure Plasma (LTAPP), which has demonstrated a significant impact on ESKAPE pathogens [2]. LTAPP is renowned for its multifaceted properties, including antimicrobial, anti-inflammatory, and tissue repair capabilities, potentially addressing several diseases [3,4].

The mechanism of LTAPP's antimicrobial action can be categorized as direct and indirect. Direct action involves the immediate application of plasma on pathogens, while the indirect mode exploits the use of liquids, primarily water, treated with plasma [4]. This indirect approach relies on the unique reactive species generated in the liquid medium due to plasma treatment. A prominent product of this indirect approach is Plasma-Activated Water (PAW) [5]. PAW is produced by exposing the water with LTAPP, boasting a diverse range of applications from degrading chemical compounds in water to facilitating environmental solutions, nanoparticle production, dispersion,

 doi:10.20944/preprints202311.0229.v1

and biological processes [6–9]. The rising interest in PAW can be attributed to the plasma's capacity to generate UV radiation and radicals, catalyzing chemical reactions in liquid mediums [10]. The unique attributes of PAW are derived from radicals and species, primarily OH and NO, generated by plasma. These radicals serve as precursors to more stable compounds such as hydrogen peroxide (H_2O_2), nitrous acid (HNO_2), and nitric acid (HNO_3) [11,12].

PAW presents a significant advantage over direct plasma jets, preventing hazards associated with electric currents, high voltages, thermal damage to tissues, and UV exposure [13]. Studies have revealed PAW's potent antimicrobial efficacy, which is attributed to the combined effects of nitrite (NO_2^-), nitrate (NO_3^-), hydrogen peroxide (H_2O_2), which are typically produced at lower pH levels [10]. With its broad-spectrum antimicrobial capabilities, ease of use, and the ability to eradicate microorganisms via non-thermal plasma discharges, PAW emerges as a promising tool in the fight against infectious diseases [14].

To further enhance the efficacy and applications of PAW, various production techniques are being explored in the field of plasma science [5]. Notable among these are the Gliding Arc and Plasma Jet techniques, which utilize electrical discharge to create non-thermal plasma under atmospheric conditions [15]. These techniques are celebrated for their energy efficiency and ability to generate reactive oxygen and nitrogen species (RONS), making them effective mediums for PAW production [16,17].

Another promising approach is the utilization of Dielectric Barrier Discharge (DBD) [18–22]. DBDs generate non-thermal plasma at atmospheric pressure and are favored for producing a uniform discharge and optimal energy density [18,19]. In a DBD setup, at least one electrode is insulated by a dielectric layer, preventing arc discharge transition and fostering a non-uniform electric field, which enables non-thermal plasma generation [19]. There are many types of DBD systems, such as planar DBD systems known for their flat electrode arrangements, which are ideal for surface treatments and film depositions. Meanwhile, packed-bed DBD and microplasma DBD systems address specific needs in pollution control and medical therapies, respectively [19].

Additionally, cylindrical DBD systems, with their coaxial electrodes, excel in promoting uniform gas flow treatments [23]. The coaxial design of DBDs allows for even gas flow treatment between coaxial cylindrical electrodes. This design makes them suitable for large-volume gas reactant treatment, such as the removal of NO_x and SO_2 from flue gas and methane reformation. These DBDs have various applications, including surface modification, materials synthesis, thin film deposition, and the activation of liquids, like PAW [24–27].

DBD can activate water by exposing it to gas effluent containing reactive species like NO_2^-, NO_3^-, O_3, H_2O_2, and other free radicals [20]. These can react with water molecules, altering their properties [27]. The effectiveness of PAW treatment depends on several factors, including the type and concentration of reactive species in the gas effluent, the exposure duration, and the composition of the water being treated [28]. The process can be optimized by adjusting DBD discharge parameters, such as voltage, frequency, and gas flow rate. The application of DBD gas effluent in water activation represents an emerging frontier in scientific research, with potential multidisciplinary applications.

In this context, the study focuses on producing PAW using a coaxial DBD reactor, with air as the working gas. This work provides a characterization of the developed system, concentrating on operational parameters. The process includes quantification of power consumption and adjustments to variables such as gas flow rate, activation interval, and volumetric parameters. An assessment of the produced PAW involved physicochemical characterization, examining parameters like pH, redox potential ORP, conductivity, Total Dissolved Solids (TDS), and concentrations of RONS. The PAW showed concentrations of reactive species and physicochemical attributes, differentiating it from systems in existing literature that require longer processing times and might not achieve these values. Additionally, the potential applications of PAW were explored using microbiological assays, assessing its effectiveness against the Gram-positive bacterium *Staphylococcus aureus*, Gram-negative bacterium *Escherichia coli*, and the fungus *Candida albicans*. The results suggest that PAW could be useful for the treatment of infectious diseases.

Preprints (www.preprints.org) | NOT PEER-REVIEWED | Posted: 3 November 2023 doi:10.20944/preprints202311.0229.v1

2. Materials and Methods

2.1. DBD reactor and electrical characterization

PAW was synthesized by exposing distilled water to the effluent gas produced by a coaxial DBD reactor [29]. This reactor consists of two concentric stainless steel tube electrodes: an inner electrode insulated by a dielectric material (silicone), which is polarized by a high-voltage source (Inergiae, ALT0215), and an outer grounded electrode (**Figure 1**). The reactor features a gas inlet positioned at the top and a gas outlet submerged within the sample. This configuration ensures an enhanced interaction between the effluent gas and the sample, optimizing liquid activation. For gas flow control, an air rotameter (Omega, FLDA3215ST) was employed.

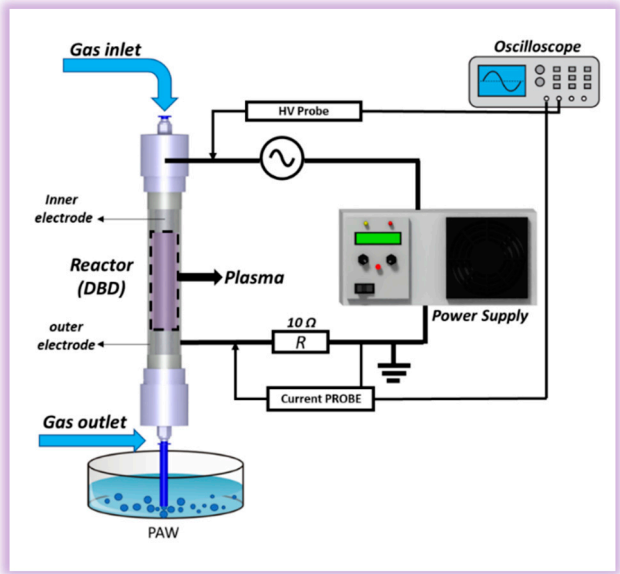

Figure 1. Schematic representation of the coaxial DBD reactor and its electrical monitoring setup [29].

Electrical signals from the DBD discharge were captured using a digital oscilloscope (Keysight DSOX1202A). A high-voltage probe (Tektronix, P6015A) was connected to the inner electrode, while a 10x voltage probe (Tektronix, TPP0051) was linked to the grounded electrode. To measure the discharge current, the voltage was assessed across a 10 Ω resistor positioned in series with the ground.

2.2. Water activation process and samples

The experimental variables are grouped into three primary categories: Volume (mL), ranging from 25 to 150 mL with increments of 25 mL; Gas Flow Rate (L/min), with values spanning from 1 to 6 L/min; and Activation Time (min), covering a spectrum from 2 to 10 minutes in two-minute steps. Each combination of these variables constitutes a distinct experimental condition for examining PAW generation. Therefore, every defined volume was tested across the complete array of activation times and gas flow rates.

The deionized (DI) water employed as the starting material exhibited the following characteristics: pH = 7.37, ORP = 19.7 mV, conductivity = 0.024 mS/cm, and TDS = 10.95 mg/L, which were determined using a Metrohm 913 pH meter.

Reactive species produced in the PAW were identified and quantified using UV-VIS spectrophotometry on the Evolution 201 UV-VIS Spectrophotometer (Thermo Scientific, USA). Deconvoluting each spectrum revealed the presence of NO_2^-, NO_3^-, H_2O_2, HNO_2, and O_3 [30,31]. Following the methodology described by Liu et al. [32], and utilizing standard concentrations of NO_2^-, NO_3^-, and H_2O_2 [32], the concentrations of Reactive Oxygen and Nitrogen Species (RONS) were

 doi:10.20944/preprints202311.0229.v1

determined based on the absorbance at wavelengths of 230 nm and 235 nm, as gleaned from the UV-VIS spectra for each experiment. In addition, test strips (Bartovation, USA) for NO_2^-, NO_3^-, and H_2O_2 were employed to quantify these species and validate the determined concentrations. With the concentration of NO_2^- defined along with pH measurements, using Equation 1 is possible to determine the concentration of HNO_2 in PAW [28,33]:

$$[HNO_2] = \frac{[NO_2^-]}{10^{pH-pKa}} \quad (1)$$

Where: $[NO_2^-]$ is the NO_2^- concentration, pH is the pH of the PAW, and pKa (3.38) is the acidity constant of HNO_2.

2.3. Microbiological assays – Assessment of antimicrobial activity of PAW

The antibacterial and antifungal efficacy of the synthesized PAW was assessed against S. aureus (ATCC 6538), E. coli (ATCC 10799), and C. albicans (SC 5314).

The microorganisms were plated on Petri dishes using Brain Heart Infusion Agar (BHI) or Saboraud Dextrose Agar, and then incubated at 37 °C for 24 h. Subsequently, standardized suspensions containing 106 cells/mL of each microbial species were prepared in a sterile saline solution (NaCl 0.9%). These suspensions were obtained using a spectrophotometer (AJX-1600, Micronal, São Paulo, SP, Brazil) adopting the following parameters: S. aureus, wavelength (λ) of 490 nm and optical density (O.D.) of 0.374; E. coli, λ = 490 nm and O.D. = 0.050; and C. albicans, λ = 530 nm and O.D. = 0.138.

The antimicrobial activity of PAW was evaluated using two distinct test groups: (a) Sterilized PAW and (b) Sterilized deionized water, which served as a negative control. Microbiological assays were conducted 40 minutes post-activation. Following the activation process, PAW samples were promptly relocated to sterile containers and stored in a sealed thermal box. This step was critical to negate potential alterations induced by environmental factors, such as ambient temperature or light. It's pertinent to note that the physicochemical properties of PAW were continuously monitored for a duration of 2 hours, which surpasses the 40-minute interval prior to microbiological testing, thus ensuring the optimal antimicrobial performance of PAW during assays.

PAW was sterilized using a 0.22 µm filter. A 250 µL aliquot of the microbial suspension was put in contact with 1,750 µL of PAW in test tubes for 10 and 30 min. After, serial dilutions of the final suspension were prepared in sterile saline solution (0.9% NaCl). An aliquot of 10 µL from each dilution was then cultured on Brain Heart Infusion (BHI) agar for S. aureus and E. coli and on Sabouraud Dextrose Agar for C. albicans.

These plates were incubated at 37 °C for 24 h and, after this period, the colonies were counted and the value of colony-forming units per milliliter (CFU/mL) was calculated. Each experiment was performed in triplicate in three different occasions (n = 9). The reduction percentage was then calculated using the Equation (3):

$$\% \text{ Reduction} = \frac{(\bar{X} \text{ CFU/mL control} - \bar{X} \text{ CFU/mL groups tested})}{\bar{X} \text{ CFU/mL control}} \text{ x } 100 \quad (2)$$

Results were analyzed and graphed using GraphPad Prism v8.0 software. The antimicrobial effects on *S. aureus* and *E. coli* were compared using a paired t-test. As the data for *C. albicans* were not normally distributed, they were compared using the Mann-Whitney's test. The significance level was set at 5%.

3. Results

3.1. Electrical characterization of coaxial DBD plasma

The voltage-current waveform of DBD air plasma is shown in **Figure 2**. The observed peak-to-peak voltage was 17.2 kV and the peak-to-peak current was 102 mA.

Preprints (www.preprints.org) | NOT PEER-REVIEWED | Posted: 3 November 2023 doi:10.20944/preprints202311.0229.v1

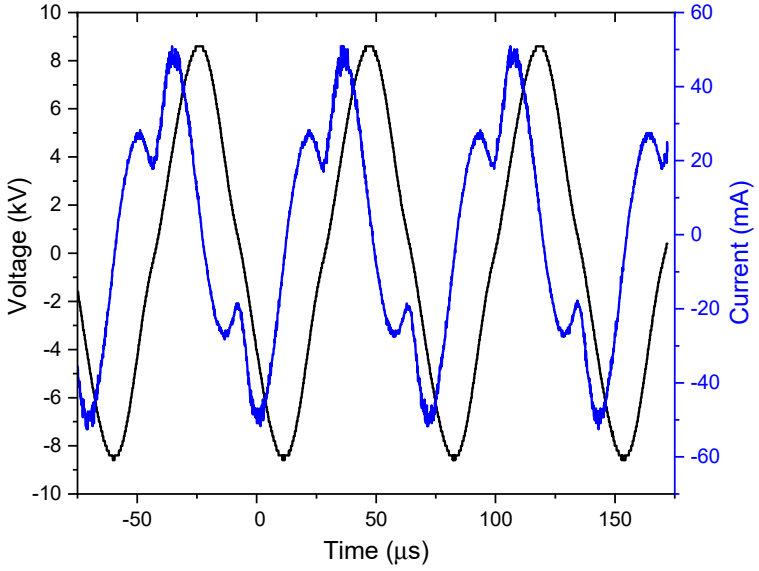

Figure 2. Voltage-current waveform of DBD air plasma.

The average power (P_m) was determined using following equation:

$$P_m = \frac{1}{T}.\int_0^T V_{plasma}(t) I_{plasma}(t) dt \quad (2)$$

The value recorded for P_m was 50.7 W. It's important to emphasize that for all the gas flow rate studied in this work, the voltage-current characteristics changed only slightly, resulting in an average plasma power of approximately (50.7 ± 1.0) W.

3.2. Coaxial DBD reactor mapping

To optimize the efficiency of the coaxial DBD reactor, we adjusted parameters including gas flow rate, activation time, and activated volume, aiming to understand their impact on liquid activation. By analyzing pH, ORP, Conductivity, TDS, and RONS concentrations, we were able to discern the effect of these variables on the chemical properties of PAW, providing insights for potential refinements.

3.3. Impact of gas flow rate on activation

Initially, we examined the influence of the gas flow rate during activation, utilizing a 25 mL volume and an activation time of 10 minutes. **Figure 3A** displays the observed pH and ORP values, whereas **Figure 3B** illustrates the conductivity and TDS measurements.

Preprints (www.preprints.org) | NOT PEER-REVIEWED | Posted: 3 November 2023 doi:10.20944/preprints202311.0229.v1

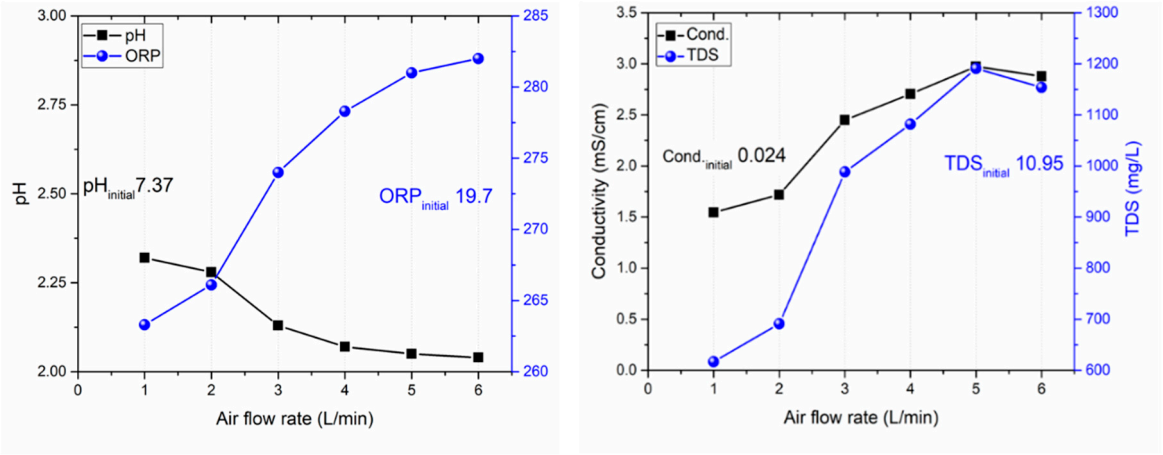

(**a**) (**b**)

Figure 3. Variation in (**a**) pH and ORP, and (**b**) Conductivity and TDS, in relation to varying air flow rates after 10 minutes of plasma activation.

The appropriate selection of gas flow rate is essential for the efficient production of RONS in the DBD plasma. These species interact with water, resulting in its acidification. A flow rate that's too low may not produce sufficient reactive species, potentially compromising the efficiency of the plasma process [10,16,34]. Data from a test at the lowest gas flow rate of 1 L/min indicates a pH of approximately 2.3, accompanied by reduced ORP (262 mV), conductivity (1.5 mS/cm), and TDS (600 mg/L) values. With an increase in gas flow rate, pH values were observed to decrease, stabilizing around 5 L/min. In parallel, conductivity and TDS values also appeared to stabilize at this rate.

In DBD plasma studies, the specific input energy (SIE) is commonly used to evaluate the power-to-gas flow rate ratio [35]. DBD systems are known for their effectiveness in ozone production and, when operated with atmospheric airflow, for generating NOx species [36]. The efficiency yield (EY) serves as a parameter to measure ozone generation efficiency. It's defined as the ratio of the ozone concentration produced during discharges to the SIE [36]. **Figure 4** displays the EY (and pH) in relation to the SIE, using data from Figure 3. An ozone meter (Ozone Solutions Inc., model UV-106 H) situated at the DBD exhaust measured the ozone concentration. The findings indicate that a superior EY is linked to a reduced SIE, suggesting a more significant airflow. Consistent with this, Yuan et al. [36] observed that for DBD systems operated in air, the concentration of NO2 peaks at a lower SIE value. Primary reactions involve the oxidation of NO by oxygen atoms, represented by the reaction $NO + O + M \rightarrow NO_2 + M$ and by ozone $NO + O_3 \rightarrow NO_2 + O_2$ [37]. However, Jogi et al. [38] noted that when the SIE exceeds 400 J/L, a modest decrease in NO_2 concentration is evident. This reduction is attributed to the reaction $NO_2 + O \rightarrow NO + O_2$, which becomes more prevalent at higher SIEs, thereby limiting the accumulation of NO_2 [38]. Understanding that water acidification through plasma-derived species predominantly engages reactive nitrogen species, this analysis aptly supports the detected pH decrease with declining SIE (or augmented airflow).

Preprints (www.preprints.org) | NOT PEER-REVIEWED | Posted: 3 November 2023 doi:10.20944/preprints202311.0229.v1

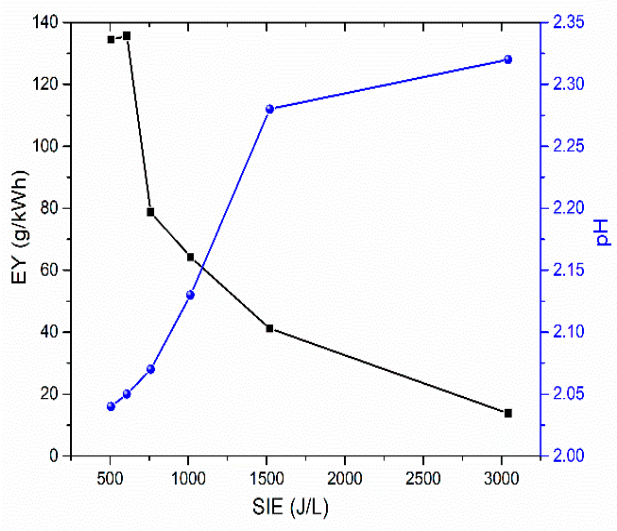

Figure 4. Ozone generation efficiency and PAW pH as a function of SIE.

Exploration of PAW is enhanced by comparing UV-VIS analysis with airflow dynamics. Through UV-VIS spectrophotometry and spectral deconvolutions, the presence of key reactive species, specifically NO_2^-, NO_3^-, H_2O_2, O_3, and HNO_2, is identified. **Figure 5** presents a comprehensive visualization of these findings.

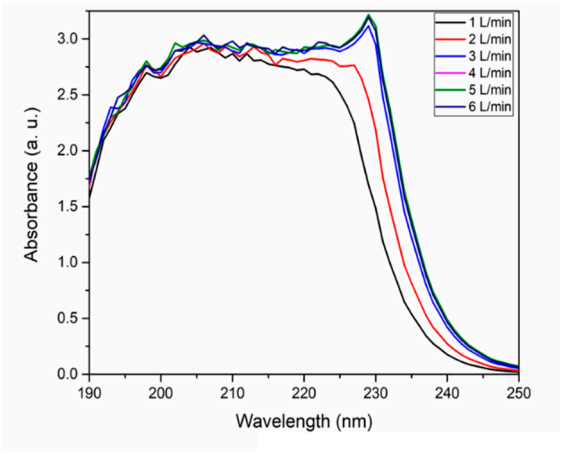

(**a**)

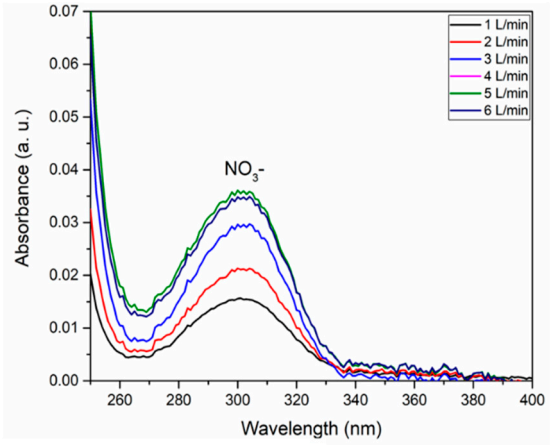

(**b**)

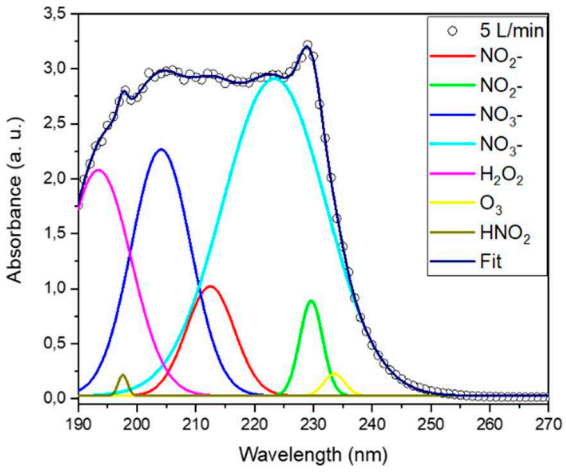

(c)

 doi:10.20944/preprints202311.0229.v1

Figure 5. UV absorption spectra of PAW at different air flow rates (from 1 to 6 L/min): (**a**) Deep UV absorption spectrum, (**b**) Near UV absorption spectrum, and (**c**) Deconvolution techniques applied for RONS identification.

Figures 5A and 5B showcase the deep and near UV absorption spectra of PAW, highlighting the pronounced impact of varying gas flow rates. The identification of reactive species such NO_2^-, NO_3^-, H_2O_2, O_3, and HNO_2 was achieved through the deconvolution of the deep UV absorption spectra, depicted in Figure 5C. These species arise from diverse reaction pathways, including both transient and persistent reactive species generated in the plasma phase [10,16]. A distinct peak around 300 nm in Figure 5B solidifies the consistent presence of NO_3^- across various gas flow rates [39].

To determine the concentrations of NO_2^-, NO_3^-, and H_2O_2, UV-VIS spectrophotometry was employed. Standard curves from Z. Liu et al. [32] provided the reference benchmarks. The alignment of band intensities from these standards with the PAW spectra, particularly at wavelengths of 230 nm and 235 nm, facilitated the precise quantification of NO_2^-, NO_3^-, and H_2O_2 in the PAWs. Cross-referencing these values with test strip results further reinforced the accuracy of the quantification approach.

Upon determining the NO_2^- concentration, nitrous acid (HNO_2) concentration can be extrapolated using Equation 1 [28,33]. As detailed by Tachibana et al. [33], the balance between HNO_2 and NO_2^- concentrations hinges on the solution's pH, considering HNO_2 has an acidity constant (pKa) of 3.38 at room temperature. Hence, the quantified concentrations of NO_2^-, NO_3^-, H_2O_2, and HNO_2 are tabulated in **Table 1**.

Table 1. Concentrations of NO_2^-, NO_3^-, H_2O_2, and HNO_2 across air flow rates ranging from 1 to 6 L/min.

Air flow rate (L/min)	NO_2^- (mg/L)	NO_3^- (mg/L)	H_2O_2 (mg/L)	HNO_2 (mg/L)
1	1.94	237.90	1.38	22.27
2	2.93	382.70	2.04	36.88
3	4.40	473.07	2.75	78.24
4	4.82	492.09	2.86	98.41
5	5.00	500.00	3.00	106.89
6	4.82	495.29	2.86	105.45

A distinct trend is observed, showcasing rising concentrations of NO_2^-, NO_3^-, and HNO_2 with gas flow, peaking notably at 5 L/min. This trend indicates the enhanced generation of these species and illustrates the relationship between airflow and chemical dynamics. These nitrogen compounds emerge as typical byproducts in PAW systems when nitrogen or air is used as the feed gas. With an increase in gas flow, a rise in NO_2^- concentration becomes evident, leading to a surge in nitrous acid under more acidic conditions. This chemical shift causes the solution to become more acidic. The spectral region between 230-280 nm, as highlighted in Figure 5B, supports O_3 presence, suggesting that ozone production is most effective at a flow rate of 5 L/min.

Additionally, the presence of ozone in PAW intensifies due to its strong oxidizing properties. Interactions with water produce reactive oxygen species (ROS), and reactions with nitrogen oxides yield reactive nitrogen species (RNS). The growing concentrations of NO_2^-, NO_3^-, and HNO_2 not only validate a significant generation of ozone but also serve as indirect indicators of the ozone yield.

Ultimately, the varying concentrations of these reactive species in PAW enhance its therapeutic and antimicrobial capabilities, triggering oxidative stress and showcasing strong antimicrobial effects across various applications [40–42].

3.4. Influence of activation time

The temporal duration of plasma exposure, commonly referred to as the activation time, significantly influences the characteristics of PAW. By modulating this time factor, it's feasible to adjust the specific activation level of PAW. This versatility broadens its application spectrum,

Preprints (www.preprints.org) | NOT PEER-REVIEWED | Posted: 3 November 2023 doi:10.20944/preprints202311.0229.v1

encompassing areas such as microbial disinfection and medicinal therapeutics [41,43,44]. Taking into account that an airflow rate of 5 L/min had previously exhibited peak performance, it was retained as the baseline for this investigative phase. A consistent volume of 25 mL was used for each test.

Figure 6A provides a visual representation of the pH and ORP values for PAW at varying activation times. Meanwhile, Figure 6B displays the results for conductivity and Total Dissolved Solids (TDS).

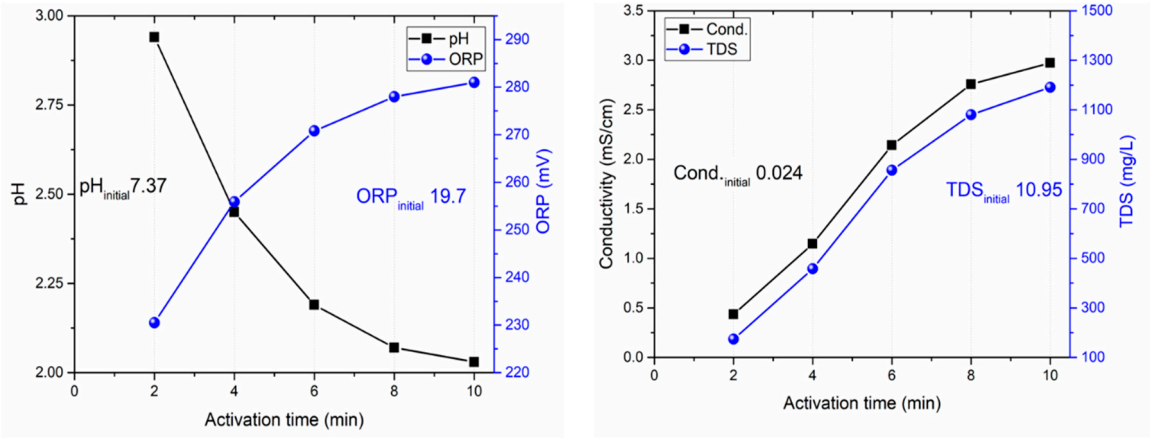

(**a**) (**b**)

Figure 6. Variation of (**a**) pH and ORP and (**b**) Conductivity and TDS with changes in activation time. Here the air flow rate was fixed in 5 L/min.

Analysis of the gathered data revealed that after a 2-minute activation, the PAW had a pH below 3, an ORP around 230 mV, conductivity at 0.5 mS/cm, and TDS at 150 mg/L. These findings are significant; for instance, a reduced pH can enhance PAW's antimicrobial capabilities [40]. A heightened ORP indicates increased oxidizing potential, bolstering PAW's effectiveness against microorganisms [45]. This elevated ORP corresponds to a more oxidizing medium that can deactivate enzymes and damage cells, effectively combating pathogens [44].

Moreover, the conductivity of PAW can influence its antimicrobial properties. The ions in the water can potentially affect microbial cell membrane permeability, aiding in the disinfection process [42]. TDS, on the other hand, may further augment PAW's antimicrobial potency; certain ions exhibit bactericidal effects, and high TDS levels can create a hostile environment for microbes, reducing their viability [45]. Notably, a consistent set of PAW parameters was achieved after 8 minutes of activation, with pH, ORP, conductivity, and TDS values stabilizing at 2.12, 276 mV, 3 mS/cm, and 1,200 mg/L, respectively.

It's worth emphasizing that these attributes arise due to the presence of Reactive Oxygen and Nitrogen Species (RONS) in PAW. To verify their presence, techniques like UV-VIS spectrophotometry, deconvolution, and various test strips for NO_2^-, NO_3^-, and H_2O_2 were employed. The outcomes are illustrated in **Figure 7**.

The absorption spectra for different activation intervals, both in the deep and near UV realms, are detailed in Figures 7A and 7B. A notable observation in the near UV spectrum (Figure 7B) is the consistent presence of NO_3^- [10,46], bearing semblance to the pattern observed with changes in gas flow rate. However, it manifests with heightened intensity around the 10-minute activation mark.

The quantification of species NO_2^-, NO_3^-, H_2O_2, and HNO_2 (**Table 2**) was conducted, revealing that as the activation time increases, the concentration of NO_2^-, NO_3^-, H_2O_2, HNO_2 also increases, reaching values of 5 mg/L for NO_2^-, 500 mg/L for NO_3^-, 3 mg/L for H_2O_2, and 106.89 for HNO_2.

Drawing a parallel to the research conducted by Laurita et al. [47], where they evaluated the concentration of specific reactive species in multiple liquids employing air DBD plasma, our findings, particularly for deionized water post a 10-minute activation, seem to be in alignment, with concentrations reaching 217 mg/L for NO_3^-, 4.6 mg/L for NO_2^-, and 10 mg/L for H_2O_2.

Preprints (www.preprints.org) | NOT PEER-REVIEWED | Posted: 3 November 2023 doi:10.20944/preprints202311.0229.v1

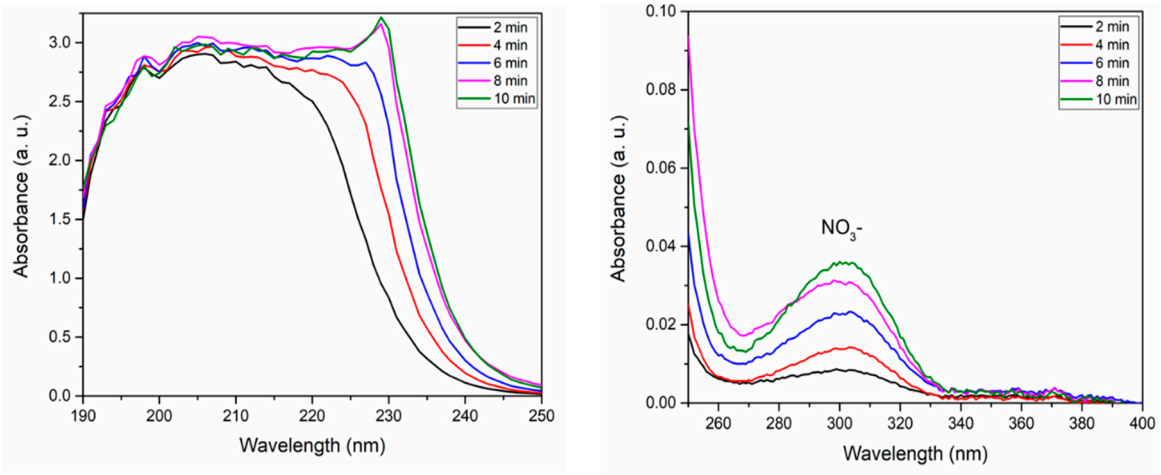

(a) (b)

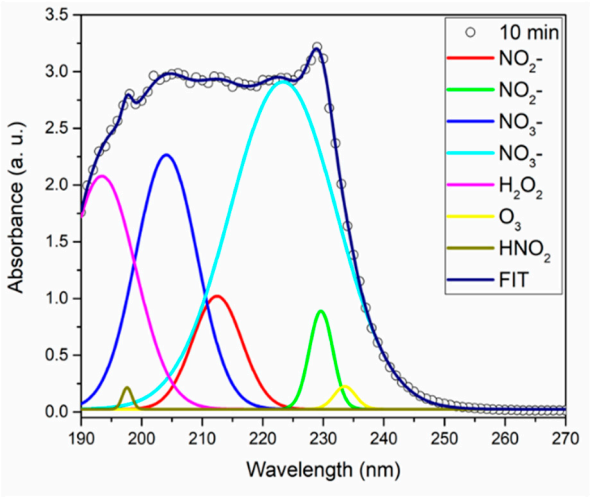

(c)

Figure 7. UV absorption spectra of PAW at various activation intervals: 2, 4, 6, 8, and 10 minutes. (**a**) Deep UV absorption spectrum, (**b**) Near UV absorption spectrum, and (**c**) Deconvolution employed for RONS identification.

Table 2. Concentrations of NO_2^-, NO_3^-, H_2O_2, and HNO_2 across activation times of 2, 4, 6, 8, and 10 minutes.

Activation time (min)	NO_2^- (mg/L)	NO_3^- (mg/L)	H_2O_2 (mg/L)	HNO_2 (mg/L)
2	1.14	133.74	0.78	3.13
4	2.03	247.27	1.44	17.53
6	3.14	366.54	2.13	48.63
8	4.51	474.26	2.76	92.08
10	5.00	500.0	3.00	106.89

3.5. Influence DI water volume

The subsequent phase of this research delved into the influence of the DI water volume on the activation process. **Figure 8A** illustrates the pH and ORP measurements, while Figure 8B depicts the data related to conductivity and total dissolved solids (TDS).

The smaller volume (25 mL) of activation results in a greater decrease in the pH and an increase in the water's Oxygen Reduction Potential (ORP). This occurs due to the concentration effect of reactive oxygen and nitrogen species (RONS) [48]. When the volume is increased, maintaining the parameters of the same reactor, the same amount of RONS is distributed, resulting in a lower

Preprints (www.preprints.org) | NOT PEER-REVIEWED | Posted: 3 November 2023 doi:10.20944/preprints202311.0229.v1

concentration of these species compared to the smaller volume. This leads to a less pronounced chemical reaction and a lower impact on the pH of the activated water, although the pH is maintained under 2.8 for all volumes. Therefore, the higher concentration of plasma species, such as reactive nitrogen species (RNS) like $NO3^-$ ions and $NO2^-$ ions in the smaller volume (25 mL) contributes to a more significant reduction in pH, reaching the value of 2.05, and higher values of ORP reaching values of 282 mV. The effect of lower pH and higher ORP assists in the antimicrobial effect of PAW [41].

The concentration effect also applies to conductivity and total dissolved solids (TDS) when considering a smaller volume of activated water. With a reduced volume, the concentration of dissolved ions and other solutes increases, leading to higher conductivity and TDS measurements. This concentration effect arises because the same amount of dissolved substances is present in a smaller volume, resulting in a more concentrated solution. Therefore, the smaller volume (25 mL) of activated water exhibits higher values of conductivity (2.97 mS/cm) and TDS (1191 mg/L) compared to the larger volume (150 mL), which reach the values of 0.618 mS/cm for conductivity and 247 mg/L for TDS, under the same plasma activation conditions. Even so, when we observe the results, it is possible to identify a tendency toward stabilization of the parameters pH, ORP, Conductivity, and TDS from the volume of 100 mL.

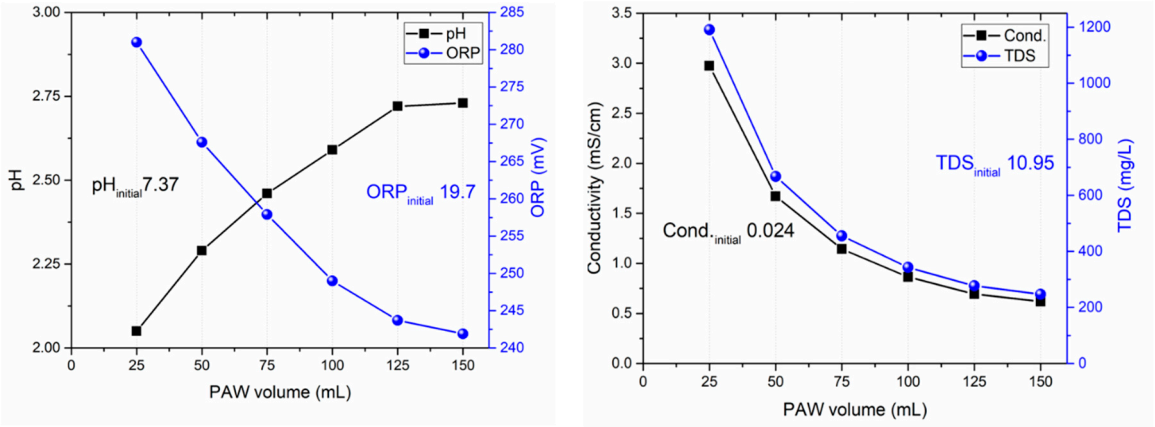

(**a**) (**b**)

Figure 8. Effects on (**a**) pH and ORP and (**b**) Conductivity and TDS at varying activation volumes. The values were obtained after 10 min plasma activation.

The characteristics of PAW concerning the concentration of RONS present in the activated volumes, characterizations were performed using UV-VIS spectrophotometry, deconvolutions, and test strips for all samples. These results are presented in **Figure 9**.

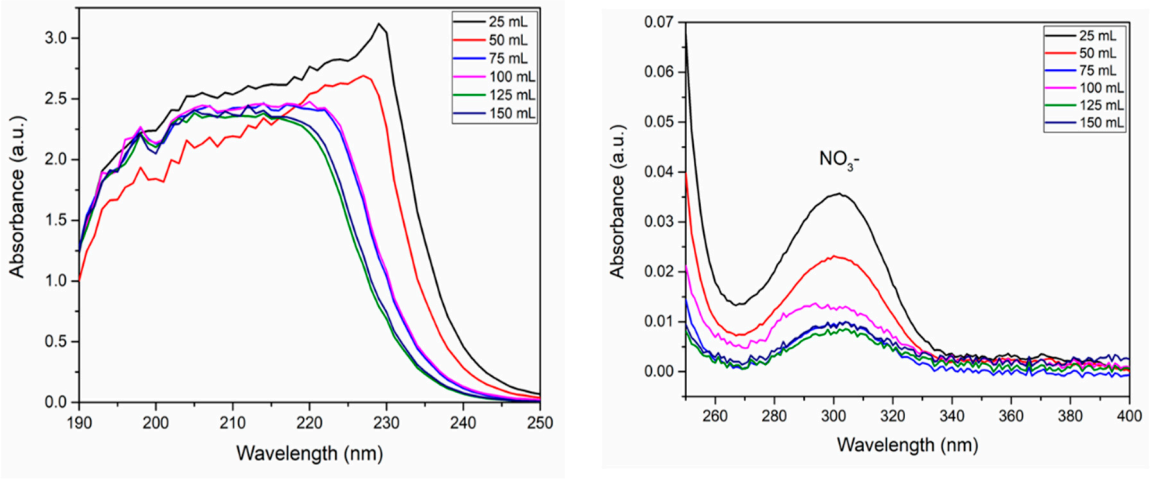

(**a**) (**b**)

Preprints (www.preprints.org) | NOT PEER-REVIEWED | Posted: 3 November 2023 doi:10.20944/preprints202311.0229.v1

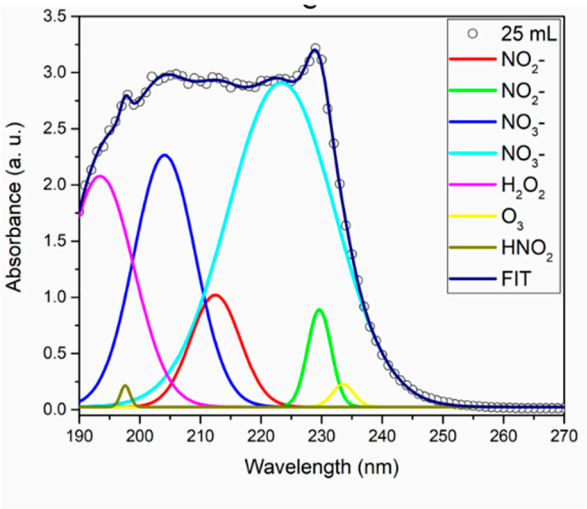

(c)

Figure 9. UV absorption spectra of PAW for PAW volume of 25, 50, 75, 100, 125, and 150 mL. (**a**) Deep UV absorption spectrum, (**b**) Near UV absorption spectrum, and (**c**) Deconvolution employed for RONS identification.

Figure 9A shows the spectra corresponding to the activation volumes studied for the deep UV absorption region. The NO_3^- is maintained, as **Figure 9B** shows near UV absorption [10,46]. For this test, a higher intensity was observed for PAW volume of 25 mL. The deconvolution (Figure 9C) of deep UV spectra was performed to identify the presence of the NO_2^-, NO_3, H_2O_2, HNO_2, and O_3. The quantification of NO_2^-, NO_3^-, H_2O_2, and HNO_2 concentrations were made and are presented in **Table 3**.

Table 3. Concentrations of NO_2^-, NO_3^-, H_2O_2, and HNO_2 at PAW volumes: 25, 50, 75, 100, 125, and 150 mL.

PAW volume (mL)	NO_2^- (mg/L)	NO_3^- (mg/L)	H_2O_2 (mg/L)	HNO_2 (mg/L)
25	5.00	500.00	3.00	106.89
50	3.06	366.23	2.11	37.64
75	1.32	166.35	0.97	10.97
100	1.40	173.84	1.01	8.63
125	0.85	110.23	0.64	3.88
150	0.92	119.05	0.69	4.11

We can note that with the increase of activation volume, the concentration of the NO_2^-, NO_3^-, and H_2O_2 decreases, which starts from 5 mg/L for NO_2^-, 500 mg/L for NO_3^-, and 3 mg/L for H_2O_2 for the volume of 25 mL and finish 1 mg/L for NO_2^-, 125 mg/L NO_3^-, 0,5 mg/L for H_2O_2.

To compare a study performed Rathore et al. [48] carried out experiments with varied activation volumes (up to 20 L), obtaining the maximum concentration values of $NO3^-$ ions, NO_2^- ions, H_2O_2, and dissolved O_3 after 10 h of plasma-water exposure were given as 93.5 mg/L, 7.5 mg/L, 4.7 mg/L, and 4.7 mg/L, respectively. Another study conducted by Oehmigen et al. [49] investigated the acidification for antimicrobial activity using a surface dielectric barrier discharge.

The experiments were carried out with variations in volume (5 and 10 mL) and activation time (10 and 30 min). The lowest pH obtained was 2.7. Additionally, the effect of volume was observed, with the higher concentration of reactive species being found for the smaller volume of 5 mL, reaching 113 mg/L for NO_3^-, 1.5 mg/L for NO_2^-, and 18 mg/L of H_2O_2. The authors also reported that the concentration of NO2- returned to 0 after 30 minutes. These results prove that for small volumes,

Preprints (www.preprints.org) | NOT PEER-REVIEWED | Posted: 3 November 2023 doi:10.20944/preprints202311.0229.v1

the concentration effect plays an important role in the quantities of the RONS in the PAW when the operational parameters of the system (reactor) were maintained the same.

3.6. Microbiological assays

The PAW evaluated in the microbiological assays was obtained under the best conditions: a flow gas rate of 5L/min, activating time of 10 min, and an activation volume of 25 mL. Under these conditions, the PAW reached the lowest pH (2.05) and higher ORP, TDS, and conductivity values. Also, higher concentrations of RONS were reached under these conditions.

The microorganisms selected for the study are significant causative agents of infections and have notable relevance due to their resistance to conventional treatments [50,51]. Moreover, they are also related to nosocomial infections. S. aureus and E. coli were chosen as representative strains of the major bacterial groups, Gram-positive and Gram-negative, respectively. C. albicans, a fungal species, was included due to its opportunistic nature and the capacity to cause a range of infections, from superficial to systemic [52].

The results of inhibition of viable cells for S. aureus, E. coli, and C. albicans are presented in **Figures 10A**, **10B** and **10C**, respectively. The exposure time for each microorganism was 10 and 30 minutes.

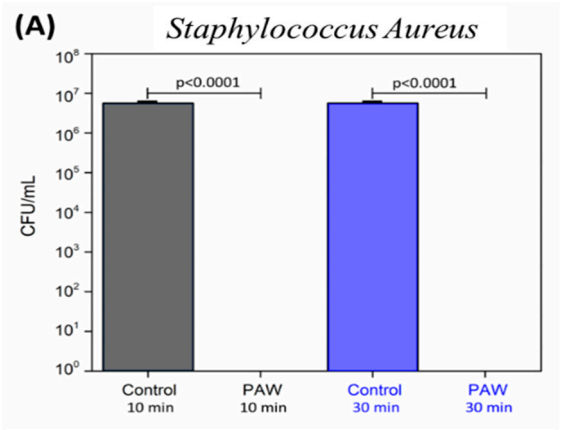

(**a**)

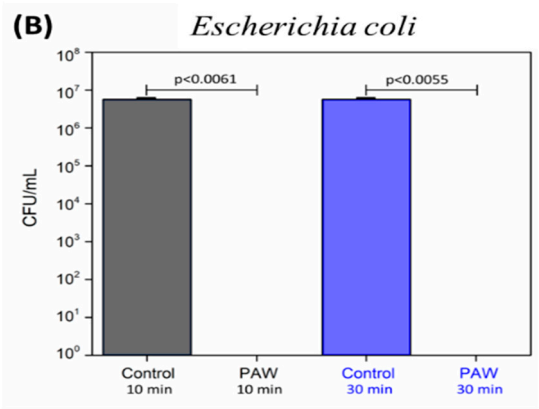

(**b**)

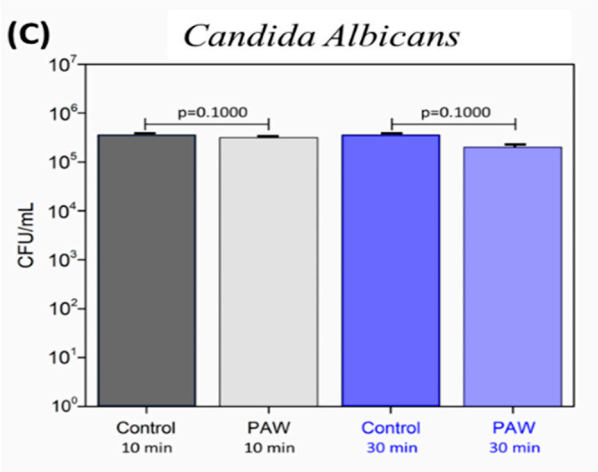

(c)

Figure 10. Number of viable cells after exposure to plasma-activated water (pH 2.05) after 10 and 30 min, where: (A) Staphylococcus aureus ATCC 6538 (CFU/mL), (B) Escherichia coli ATCC 10799 (CFU/mL), and (C) Candida albicans SC 5314 (CFU/mL). Control: non-activated deionized water (negative control).

 doi:10.20944/preprints202311.0229.v1

The exposure to PAW (pH=2.05), both for 10 and 30 minutes significantly reduced the viability of S. aureus (Figure 10A) compared to the control (pH=7.37). A total inhibition of viable cells (99.99% of reduction) was obtained for both exposure times ($p<0.0001$ and $p=0.0017$, respectively).

For E. coli (Figure 10B), there was also a significant reduction in CFU/mL with no recovery of viable cells (99.99% reduction) after both 10 and 30 min to PAW (pH=2.05) of contact ($p=0.0061$ and $p=0.0055$, respectively), compared to the control group (pH=7.37).

Based on these results, a significant reduction in CFU/mL was observed for both S. aureus and E. coli. Although Gram-positive bacteria tend to be less susceptible to non-thermal plasma jet [2], this feature was not observed for PAW, probably due to the different reactive species formed in PAW. The different reactive species may act differently on the microbial cell structures. According to Zhao et al. [41], in Gram-negative bacteria, the action of reactive species of PAW occurs in the cell wall. In contrast, in Gram-positive bacteria, they act on intracellular components, causing damage that leads to the process of cell death.

The effects of low pH and the concentrations of reactive species present in water, such as NO_2^-, NO_3^-, and H_2O_2, activated by plasma, are of fundamental significance in the inactivation or demise of microorganisms, as these species damage their cellular membranes and components. In these contexts, Zhang et al. [21] reported a study on the inactivation of Staphylococcus aureus using atmospheric helium dielectric barrier discharge. The treatment was conducted in the gas-liquid phase for different durations. Following discharge treatments lasting 1, 3, 5, and 8 minutes, the initial damage resulted in residual bacterial inactivation rates of 9.3%, 37.2%, 81.8%, and 86.7%, respectively. In this study the pH values did not fall below 4.0, and the concentrations of NO_3^- and H_2O_2 were approximately 20 mg/L and 90 mg/L, respectively. Although H_2O_2 is an effective agent against microorganisms, it alone is not capable of achieving complete microbial reduction, as explained in the current study [53].

Another study conducted by Zhou et al. [54] is a comparative investigation involving Plasma-Activated Water (PAW) and a solution containing an equivalent concentration of reactive species to those present in PAW, for the treatment of Escherichia coli. The application of PAW resulted in a reduction exceeding 4 logarithmic units, whereas exposure to an equivalent single dose of hydrogen peroxide (H_2O_2), nitrate (NO_3^-), or nitrite (NO_2^-) failed to attain a similar level of reduction. Remarkably, peroxynitrite emerged as a pivotal bioactive species, particularly under acidic conditions, originating from the synergistic plasma effects, including the reactions of H_2O_2, NO_3^-, NO_2^-, and other short-lived species like OH radicals within PAW.

Following the discussion of the results of the present study, for C. albicans (Figure 10C), after a 10-minute contact with plasma-activated water (PAW), a reduction percentage of 12.05% ($p=0.1000$) was achieved when compared to the control group (pH=7.37). After 30 minutes of exposure, the reduction percentage was 37.50% ($p=0.1000$). However, the decrease in CFU/mL observed did not show statistical significance.

Fungal cells seem to be more resistant to plasma activated liquids when compared to bacteria, probably due to their more complex cell structure. No significant reduction in cell viability when C. albicans was exposed to tap water activated by plasma generated in a gliding arc system (pH 3.5). The association between LTAPP and PAW has been recently suggested to improve the effectiveness against fungal species and should be evaluated in future studies [55]. According to Sherrington et al. [56], C. albicans can survive in environments with a pH ranging from 2 to 10, as it can colonize sites such as the stomach, vagina, and oral mucosa in the host. Further studies exploring the efficacy of PAW against this fungus are still necessary. When compared to bacterial cells, C. albicans exhibits different characteristics and virulence factors, which can also vary among clinically relevant strains belonging to the same genus and species [52].

4. Conclusions

This study methodically determined the optimal operating conditions for a coaxial DBD reactor in producing high-quality PAW. It was observed that DBD discharges, when facilitated with an air flow, exhibited an elevated capacity to produce PAW with substantial concentrations of nitrogen-

based species. Through the manipulation of gas flow rate, activation time, and volume, the best conditions were identified. The prime conditions consisted of a gas flow rate of 5 L/min, an activation time of 10 min, and a PAW volume of 25 mL. Under these parameters, there was a pronounced elevation in the concentrations of NO_2^-, NO_3^-, H_2O_2, and HNO_2. The resulting PAW possessed distinct physicochemical properties such as a pH of 2.06, an ORP of 275mV, conductivity of 3mS/cm, and TDS of 1200 mg/L. Furthermore, the assessments of SIE and EY played a pivotal role in this research. These metrics reflected the efficiency of the DBD reactor in terms of energy input and the corresponding yield, solidifying its potential for sustainable PAW production. In terms of antimicrobial potency, the PAW demonstrated significant efficacy. The viability of both Gram-positive (*S. aureus*) and Gram-negative (*E. coli*) bacteria saw a substantial reduction, while the fungus C. albicans showed a more moderate decline in viability. In conclusion, the coaxial DBD reactor stands out as a promising tool for crafting high-quality PAW with notable antimicrobial properties. This study underscores the importance of further research to confirm the safety and broad-spectrum applications of PAW, while also emphasizing the potential of optimizing the DBD method, especially in the context of energy efficiency and yield via SIE and EY metrics.

Author Contributions: Conceptualization, F.M., R.S., and C.K.-I.; methodology, F.M., V.K.F.T., M.P.G., N. F. A. N., R.S., and C.K.-I.; formal analysis, F.M., V.K.F.T, G.P. R.S., and C.K.-I; investigation, F.M., V.K.F.T., M.P.G., R.S., and C.K.-I.; resources, F.M, C.K-I, W.C, R.P.; writing—original draft preparation, F.M., N. F. A. N.,G.P., R.S., and C.K.-I.; writing—review and editing, F.M., G.P., R.S., W.C., and C.K.-I.; supervision, R.P. and C.K.-I.; project administration, F.M., R.S., and C.K.-I.; funding acquisition, F.M., G.P., R.S., W.C., and C.K.-I. All authors have read and agreed to the published version of the manuscript.

Funding: Please add: "This research was funded by The São Paulo Research Foundation (FAPESP) (Individual Grant No. 2021/14181-3) and by the financial support of the Brazilian agency program FAPESP (Grant No. 19/05856-7).

Data Availability Statement: The data that support the findings of this study are available from the corresponding author upon reasonable request

Conflicts of Interest: The authors declare no conflict of interest.

References

1. Pulingam, T.; Parumasivam, T.; Gazzali, A.M.; Sulaiman, A.M.; Chee, J.Y.; Lakshmanan, M.; Chin, C.F.; Sudesh, K. Antimicrobial Resistance: Prevalence, Economic Burden, Mechanisms of Resistance and Strategies to Overcome. *European Journal of Pharmaceutical Sciences* 2022, *170*.
2. Scholtz, V.; Vaňková, E.; Kašparová, P.; Premanath, R.; Karunasagar, I.; Julák, J. Non-Thermal Plasma Treatment of ESKAPE Pathogens: A Review. *Front Microbiol* 2021, *12*.
3. Weltmann, K.D.; Von Woedtke, T. Plasma Medicine - Current State of Research and Medical Application. *Plasma Phys Control Fusion* **2017**, *59*, doi:10.1088/0741-3335/59/1/014031.
4. Akan, T.; Çabuk, A. Indirect Plasma Inactivation by a Low Temperature Atmospheric Pressure Plasma (LTAPP) System. *J Electrostat* **2014**, *72*, 218–221, doi:10.1016/j.elstat.2014.03.007.
5. Wong, K.S.; Chew, N.S.L.; Low, M.; Tan, M.K. Plasma-Activated Water: Physicochemical Properties, Generation Techniques, and Applications. *Processes* 2023, *11*.
6. Magureanu, M.; Piroi, D.; Mandache, N.B.; David, V.; Medvedovici, A.; Bradu, C.; Parvulescu, V.I. Degradation of Antibiotics in Water by Non-Thermal Plasma Treatment. *Water Res* **2011**, *45*, 3407–3416, doi:10.1016/j.watres.2011.03.057.
7. Magureanu, M.; Piroi, D.; Mandache, N.B.; David, V.; Medvedovici, A.; Parvulescu, V.I. Degradation of Pharmaceutical Compound Pentoxifylline in Water by Non-Thermal Plasma Treatment. *Water Res* **2010**, *44*, 3445–3453, doi:10.1016/j.watres.2010.03.020.
8. Gerrity, D.; Stanford, B.D.; Trenholm, R.A.; Snyder, S.A. An Evaluation of a Pilot-Scale Nonthermal Plasma Advanced Oxidation Process for Trace Organic Compound Degradation. *Water Res* **2010**, *44*, 493–504, doi:10.1016/j.watres.2009.09.029.
9. Locke, B.R.; Sato, M.; Sunka, P.; Hoffmann, M.R.; Chang, J.S. Electrohydraulic Discharge and Nonthermal Plasma for Water Treatment. *Ind Eng Chem Res* **2006**, *45*, 882–905, doi:10.1021/ie050981u.
10. Laurita, R.; Barbieri, D.; Gherardi, M.; Colombo, V.; Lukes, P. Chemical Analysis of Reactive Species and Antimicrobial Activity of Water Treated by Nanosecond Pulsed DBD Air Plasma. *Clin Plasma Med* **2015**, *3*, 53–61, doi:10.1016/j.cpme.2015.10.001.

11. Kamgang-Youbi, G.; Herry, J.M.; Bellon-Fontaine, M.N.; Brisset, J.L.; Doubla, A.; Naïtali, M. Evidence of Temporal Postdischarge Decontamination of Bacteria by Gliding Electric Discharges: Application to Hafnia Alvei. *Appl Environ Microbiol* **2007**, *73*, 4791–4796, doi:10.1128/AEM.00120-07.
12. Addou, A.; Brisset, J.L.; Doubla, A.; Abdelmalek, F.; Khe, K. Post-Discharge Plasma-Chemical Oxidation of Iron (II) Complexes. **2003**, 73–77.
13. Ercan, U.K.; Wang, H.; Ji, H.; Fridman, G.; Brooks, A.D.; Joshi, S.G. Nonequilibrium Plasma-Activated Antimicrobial Solutions Are Broad-Spectrum and Retain Their Efficacies for Extended Period of Time. *Plasma Processes and Polymers* **2013**, *10*, 544–555, doi:10.1002/ppap.201200104.
14. Ursache, M.; Moraru, R.; Hnatiuc, E.; Nastase, V.; Mares, M. Comparative Assessment of the Relation between Energy Consumption and Bacterial Burden Reduction Using Plasma Activated Water. *2014 International Conference on Optimization of Electrical and Electronic Equipment, OPTIM 2014* **2014**, 1036–1041, doi:10.1109/OPTIM.2014.6850972.
15. Koga-Ito, C.Y.; Kostov, K.G.; Miranda, F.S.; Milhan, N.V.M.; Azevedo Neto, N.F.; Nascimento, F.; Pessoa, R.S. Cold Atmospheric Plasma as a Therapeutic Tool in Medicine and Dentistry. *Plasma Chemistry and Plasma Processing* 2023.
16. Burlica, R.; Kirkpatrick, M.J.; Locke, B.R. Formation of Reactive Species in Gliding Arc Discharges with Liquid Water. *J Electrostat* **2006**, *64*, 35–43, doi:10.1016/j.elstat.2004.12.007.
17. Pawłat, J.; Terebun, P.; Kwiatkowski, M.; Tarabová, B.; Kovaľová, Z.; Kučerová, K.; Machala, Z.; Janda, M.; Hensel, K. Evaluation of Oxidative Species in Gaseous and Liquid Phase Generated by Mini-Gliding Arc Discharge. *Plasma Chemistry and Plasma Processing* **2019**, doi:10.1007/s11090-019-09974-9.
18. France, P.I. V; Abb, E. Dielectric-Barrier Discharges. Principle and Applications. **1997**, *7*.
19. U. Konelschatz, B.E. and W.E.A. Dielectric-Barrier Discharges. Principle and Applications. *J. PHYS IV FRANCE 7* **1997**, *7*.
20. Tang, Q.; Jiang, W.; Cheng, Y.; Lin, S.; Lim, T.M.; Xiong, J. Generation of Reactive Species by Gas-Phase Dielectric Barrier Discharges. *Ind Eng Chem Res* **2011**, *50*, 9839–9846, doi:10.1021/ie200039w.
21. Zhang, Z.; Xu, Z.; Cheng, C.; Wei, J.; Lan, Y.; Ni, G.; Sun, Q.; Qian, S.; Zhang, H.; Xia, W.; et al. Bactericidal Effects of Plasma Induced Reactive Species in Dielectric Barrier Gas–Liquid Discharge. *Plasma Chemistry and Plasma Processing* 2017, *37*, 415–431.
22. Miranda, F.S.; Rabelo, S.C.; Pradella, J.G.C.; Carli, C. Di; Petraconi, G.; Maciel, H.S.; Pessoa, R.S.; Vieira, L. Plasma In-Liquid Using Non-Contact Electrodes: A Method of Pretreatment to Enhance the Enzymatic Hydrolysis of Biomass. *Waste Biomass Valorization* **2019**, doi:10.1007/s12649-019-00824-5.
23. Liu, H.; Zhao, Y.; Zhou, Y.; Chang, L.; Zhang, J. Removal of Gaseous Elemental Mercury by Modified Diatomite. *Science of the Total Environment* **2019**, *652*, 651–659, doi:10.1016/j.scitotenv.2018.10.291.
24. Jeong, J.; Jurng, J. Removal of Gaseous Elemental Mercury by Dielectric Barrier Discharge. *Chemosphere* **2007**, *68*, 2007–2010, doi:10.1016/j.chemosphere.2007.01.044.
25. Chen, Z.; Mannava, D.P.; Mathur, V.K. Mercury Removal in Flue Gases by Dielectric Barrier Discharge Technique. *AIChE Annual Meeting, Conference Proceedings* **2004**, 7101–7104.
26. Wright, A.; Bandulasena, H.; Ibenegbu, C.; Leak, D.; Holmes, T.; Zimmerman, W.; Shaw, A.; Iza, F. Dielectric Barrier Discharge Plasma Microbubble Reactor for Pretreatment of Lignocellulosic Biomass. *AIChE Journal* **2018**, *64*, 3803–3816, doi:10.1002/aic.16212.
27. Mohades, S.; Lietz, A.M.; Kushner, M.J. Generation of Reactive Species in Water Film Dielectric Barrier Discharges Sustained in Argon, Helium, Air, Oxygen and Nitrogen. *J Phys D Appl Phys* **2020**, *53*, doi:10.1088/1361-6463/aba21a.
28. Sampaio, A. da G.; Chiappim, W.; Milhan, N.V.M.; Botan Neto, B.; Pessoa, R.; Koga-Ito, C.Y. Effect of the PH on the Antibacterial Potential and Cytotoxicity of Different Plasma-Activated Liquids. *Int J Mol Sci* **2022**, *23*, doi:10.3390/ijms232213893.
29. Miranda, F.S.; Koga-Ito, C.Y.; Pessoa, R.S.; Petraconi, G. Processo Contínuo de Tratamento e Ativação de Líquidos Nebulizado Ou de Fluxo Corrente Empregando Um Sistema de Células de Descargas Por Barreira Dielétrica 2023, 1–15.
30. Oh, J.S.; Szili, E.J.; Ogawa, K.; Short, R.D.; Ito, M.; Furuta, H.; Hatta, A. UV-Vis Spectroscopy Study of Plasma-Activated Water: Dependence of the Chemical Composition on Plasma Exposure Time and Treatment Distance. *Jpn J Appl Phys* **2018**, *57*, doi:10.7567/JJAP.57.0102B9.
31. Gamaleev, V.; Iwata, N.; Oh, J.S.; Hiramatsu, M.; Ito, M. Development of an Ambient Air Flow Rotating Arc Jet for Low-Temperature Treatment. *IEEE Access* **2019**, *7*, 93100–93107, doi:10.1109/ACCESS.2019.2928419.
32. Liu, Z.; Zhou, C.; Liu, D.; He, T.; Guo, L.; Xu, D.; Kong, M.G. Quantifying the Concentration and Penetration Depth of Long-Lived RONS in Plasma-Activated Water by UV Absorption Spectroscopy. *AIP Adv* **2019**, *9*, doi:10.1063/1.5037660.
33. Tachibana, K.; Nakamura, T. Examination of UV-Absorption Spectroscopy for Analysis of O3, NO2-, and HNO2 Compositions and Kinetics in Plasma-Activated Water. *Jpn J Appl Phys* **2020**, *59*, doi:10.35848/1347-4065/ab86fd.

34. Dharini, M.; Jaspin, S.; Mahendran, R. Cold Plasma Reactive Species: Generation, Properties, and Interaction with Food Biomolecules. *Food Chem* 2023, *405*.
35. Huang, X.; Zhou, S.; Liu, M. Investigation of the Coupled Volume Dielectric Barrier Discharge for Ozone Formation in Open Atmospheric Air. *IEEE Transactions on Plasma Science* **2018**, *46*, 2887–2893, doi:10.1109/TPS.2018.2847285.
36. Yuan, D.; Wang, Z.; He, Y.; Xie, S.; Lin, F.; Zhu, Y.; Cen, K. Ozone Production with Dielectric Barrier Discharge from Air: The Influence of Pulse Polarity. *Ozone Sci Eng* **2018**, *40*, 494–502, doi:10.1080/01919512.2018.1476127.
37. Guo, Y.; Liao, X.; Fu, M.; Huang, H.; Ye, D. Toluene Decomposition Performance and NOx By-Product Formation during a DBD-Catalyst Process. *J Environ Sci (China)* **2015**, *28*, 187–194, doi:10.1016/j.jes.2014.06.048.
38. Jõgi, I.; Erme, K.; Levoll, E.; Stamate, E. Radical Production Efficiency and Electrical Characteristics of a Coplanar Barrier Discharge Built by Multilayer Ceramic Technology. *J Phys D Appl Phys* **2017**, *50*, doi:10.1088/1361-6463/aa8dab.
39. Fateev, A.; Egsgaard, H.; Fateev, A.; Leipold, F.; Kusano, Y.; Stenum, B.; Egsgaard, H.; Bindslev, H. *Reduction of NO x by Plasma-Assisted Methods INCOM-Industrial Production Processes for Nanoreinforced Composite Structures View Project EMPIR Joint Research Project EMPRESS-"Enhancing Process Efficiency through Improved Temperature Measurement" View Project Reduction of NO x by Plasma-Assisted Methods*;
40. Traylor, M.J.; Pavlovich, M.J.; Karim, S.; Hait, P.; Sakiyama, Y.; Clark, D.S.; Graves, D.B. Long-Term Antibacterial Efficacy of Air Plasma-Activated Water. *J Phys D Appl Phys* **2011**, *44*, doi:10.1088/0022-3727/44/47/472001.
41. Zhao, Y.M.; Ojha, S.; Burgess, C.M.; Sun, D.W.; Tiwari, B.K. Inactivation Efficacy of Plasma-Activated Water: Influence of Plasma Treatment Time, Exposure Time and Bacterial Species. *Int J Food Sci Technol* **2021**, *56*, 721–732, doi:10.1111/ijfs.14708.
42. Kamgang-Youbi, G.; Herry, J.M.; Meylheuc, T.; Brisset, J.L.; Bellon-Fontaine, M.N.; Doubla, A.; Naïtali, M. Microbial Inactivation Using Plasma-Activated Water Obtained by Gliding Electric Discharges. *Lett Appl Microbiol* **2009**, *48*, 13–18, doi:10.1111/j.1472-765X.2008.02476.x.
43. Bălan, G.G.; Roşca, I.; Ursu, E.L.; Doroftei, F.; Bostănaru, A.C.; Hnatiuc, E.; Năstasă, V.; Şandru, V.; Ştefănescu, G.; Trifan, A.; et al. Plasma-Activated Water: A New and Effective Alternative for Duodenoscope Reprocessing. *Infect Drug Resist* **2018**, *11*, 727–733, doi:10.2147/IDR.S159243.
44. Zhao, Y.M.; Patange, A.; Sun, D.W.; Tiwari, B. Plasma-Activated Water: Physicochemical Properties, Microbial Inactivation Mechanisms, Factors Influencing Antimicrobial Effectiveness, and Applications in the Food Industry. *Compr Rev Food Sci Food Saf* **2020**, *19*, 3951–3979, doi:10.1111/1541-4337.12644.
45. Rathore, V.; Patel, D.; Butani, S.; Nema, S.K. Investigation of Physicochemical Properties of Plasma Activated Water and Its Bactericidal Efficacy. *Plasma Chemistry and Plasma Processing* **2021**, *41*, 871–902, doi:10.1007/s11090-021-10161-y.
46. Judée, F.; Simon, S.; Bailly, C.; Dufour, T. Plasma-Activation of Tap Water Using DBD for Agronomy Applications: Identification and Quantification of Long Lifetime Chemical Species and Production/Consumption Mechanisms. *Water Res* **2018**, *133*, 47–59, doi:10.1016/j.watres.2017.12.035.
47. Laurita, R.; Barbieri, D.; Gherardi, M.; Colombo, V.; Lukes, P. Chemical Analysis of Reactive Species and Antimicrobial Activity of Water Treated by Nanosecond Pulsed DBD Air Plasma. *Clin Plasma Med* **2015**, *3*, 53–61, doi:10.1016/j.cpme.2015.10.001.
48. Rathore, V.; Patil, C.; Kumar Nema, S. *Title: Continuous Production for Large Quantity Plasma Activated Water Using Multiple Plasma Device Setup*;
49. Oehmigen, K.; Hähnel, M.; Brandenburg, R.; Wilke, C.; Weltmann, K.D.; Von Woedtke, T. The Role of Acidification for Antimicrobial Activity of Atmospheric Pressure Plasma in Liquids. *Plasma Processes and Polymers* **2010**, *7*, 250–257, doi:10.1002/ppap.200900077.
50. da Silva, G.J.; Mendonça, N. Association between Antimicrobial Resistance and Virulence in Escherichia Coli. *Virulence* 2012, *3*, 18–28.
51. Cheung, G.Y.C.; Bae, J.S.; Otto, M. Pathogenicity and Virulence of Staphylococcus Aureus. *Virulence* 2021, *12*, 547–569.
52. Lee, Y.; Puumala, E.; Robbins, N.; Cowen, L.E. Antifungal Drug Resistance: Molecular Mechanisms in Candida Albicans and Beyond. *Chem Rev* 2021, *121*, 3390–3411.
53. Traylor, M.J.; Pavlovich, M.J.; Karim, S.; Hait, P.; Sakiyama, Y.; Clark, D.S.; Graves, D.B. Long-Term Antibacterial Efficacy of Air Plasma-Activated Water. *J Phys D Appl Phys* **2011**, *44*, doi:10.1088/0022-3727/44/47/472001.
54. Zhou, R.; Zhou, R.; Prasad, K.; Fang, Z.; Speight, R.; Bazaka, K.; Ostrikov, K. Cold Atmospheric Plasma Activated Water as a Prospective Disinfectant: The Crucial Role of Peroxynitrite. *Green Chemistry* **2018**, *20*, 5276–5284, doi:10.1039/c8gc02800a.

55. Xu, H.; Liu, C.; Huang, Q. Enhance the Inactivation of Fungi by the Sequential Use of Cold Atmospheric Plasma and Plasma-Activated Water: Synergistic Effect and Mechanism Study. *Chemical Engineering Journal* **2023**, *452*, doi:10.1016/j.cej.2022.139596.
56. Sherrington, S.L.; Sorsby, E.; Mahtey, N.; Kumwenda, P.; Lenardon, M.D.; Brown, I.; Ballou, E.R.; MacCallum, D.M.; Hall, R.A. Adaptation of Candida Albicans to Environmental PH Induces Cell Wall Remodelling and Enhances Innate Immune Recognition. *PLoS Pathog* **2017**, *13*, doi:10.1371/journal.ppat.1006403.